Supplementary Information

Molten salt modulation of porous MoP@PC nanosheets as an ultra-stable anode for lithium ion battery

Yiran Li[a†], Xinchang Geng[a†], Junhui Cai[a], Chunmei Tan[a], Yanjuan Li[a*] and Xiao Yan[a*]

[a]Jiangsu Key Laboratory of Green Synthetic Chemistry for Functional Materials, School of Chemistry & Materials Science, Jiangsu Normal University, Xuzhou, 221116, China

*Corresponding author (email: liyanjuan21@jsnu.edu.cn, yanxiao@jsnu.edu.cn)

[†]These authors contributed equally to this work

Experimental section:

Preparation of materials

Experimental section: Typical synthesis of MoP@PC-MS samples: A mixture of 0.5 g MoO_3, 1.0 g $(NH_4)_2HPO_4$ (P/Mo = 2.2), 0.88 g $C_6H_{12}O_6$ (C/Mo = 8.5), 2.75 g KCl and 2.25 g NaCl was grinded for 30 minutes until the powder is uniformly colored and finely particulated. The mixed solid powder is then placed in a tube furnace filled with Ar and maintained at 900°C for 4 hours, with a heating rate of 5°C min^{-1}. After sintering, the powder changes from ash-gray to black. The sintered sample is then uniformly stirred in a water bath at 70°C for 10 hours to remove the residual KCl and NaCl from the reaction. Following desalination, the sample is washed with DI and ethanol, and finally dried in a vacuum oven at 60°C, yielding the target product MoP@PC-MS. Carbon content is controlled by adjusting the amount of $C_6H_{12}O_6$, with C/Mo= 0, 7 and 10, and corresponding samples were denoted as MoP@PC-MS-0, MoP@PC-MS-1, and MoP@PC-MS-2, respectively.

The sample synthesized without molten salt was named as MoP@PC, in which the C/Mo is 8.5.

Material characterization:

The material phase composition of the sample was determined by X-ray diffractometer (D8). The specific content of the elements in the sample was done by Inductive Coupled Plasma Emission Spectrometer testing (ICP). The morphology and microstructure were further observed by SEM/EDS, SU-8010 and TEM, Tacnai F20. Carbon content of MoP/P-C and MoP@TiO2/P-C was determined at 25-900 °C by thermogravimetric instrument (TGA, TA-Q50). The surface elemental valence components of samples were recorded by X-ray photoelectron spectroscopy (XPS). Raman spectra were obtained using the Nd line as a laser source (lambda = 514 nm).

Electrochemical measurements:

Electrochemical performance was tested by CR-2032 coin cells assembled from working electrodes, reference electrodes, separator and electrolytes. The working electrode was prepared by grinding the electrode material (70w%), Super P (20wt%), and polyvinylidene fluoride binder (PVDF, 10wt%) in a moderate amount of N-methyl-2-pyrrolidone (NMP) to form a uniform, smooth slurry, which was then coated with copper foil collector fluid. After 12 h drying in a vacuum oven at 120 ° C, the working electrode is then pressurized under 10 MPa and then cut into 10 mm diameter poles with a load mass of 1-2 mg cm^{-2} of active material. Lithium wafers with 14 mm diameter were used as reference electrodes. Celgard 2400 with a diameter of 12 mm was used as the battery separator. The lithium ion battery electrolyte was 1.0 M $LiPF_6$ dissolved in a mixture of ethylene carbonate (EC), diethyl carbonate (DEC) and fluoroethylene carbonate (FEC) (volume ratio 6:3:1).

Charge/discharge testing was performed on a cell tester (Novavax, China) with a voltage range of 0.01-3.0 V (vs. Li/Li^+). CT2001A cell equipment (Wuhan LAND) was used for GITT testing at 0.1 A g^{-1} current density. The cyclic voltammetry (CV) test and electrochemical impedance spectroscopy (EIS) test were performed using CHI 600E electrochemical workstations with voltage ranges of 0.01-3.0 V and scanning rates of 0.1-1.0 mV s^{-1}. The EIS profile was measured at frequencies ranging from 0.01 Hz to 100 KHz.

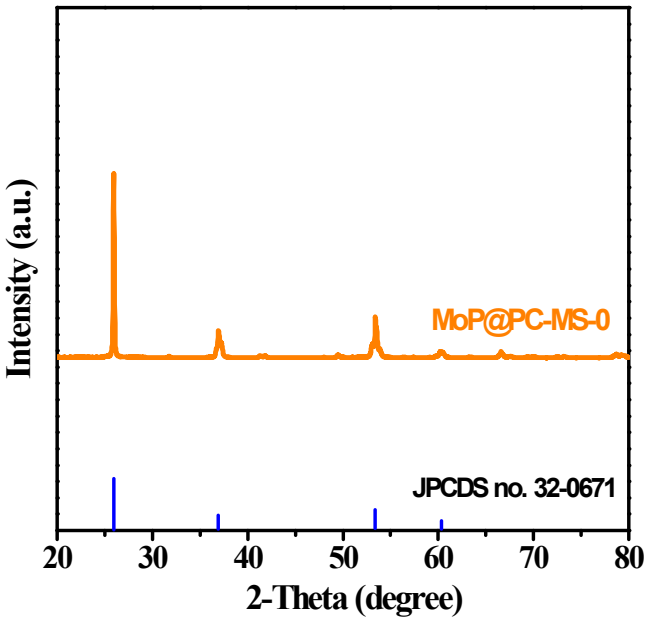

Figure S1. XRD pattern of MoP@PC-MS-0.

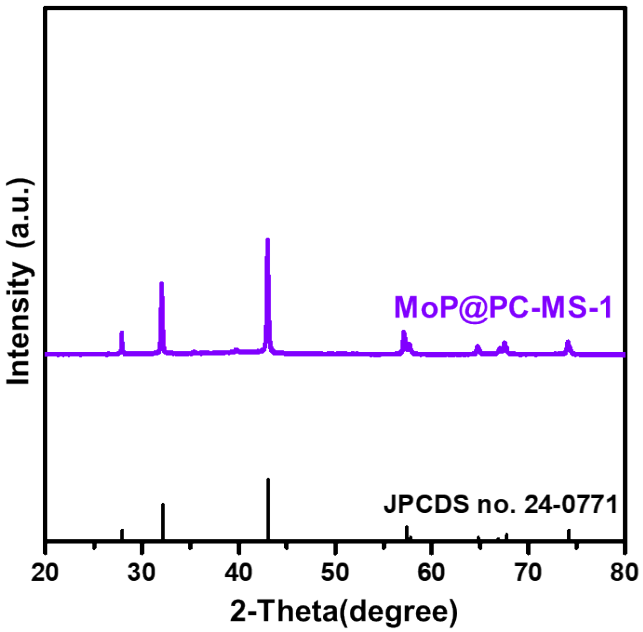

Figure S2. XRD pattern of MoP@PC-MS-1.

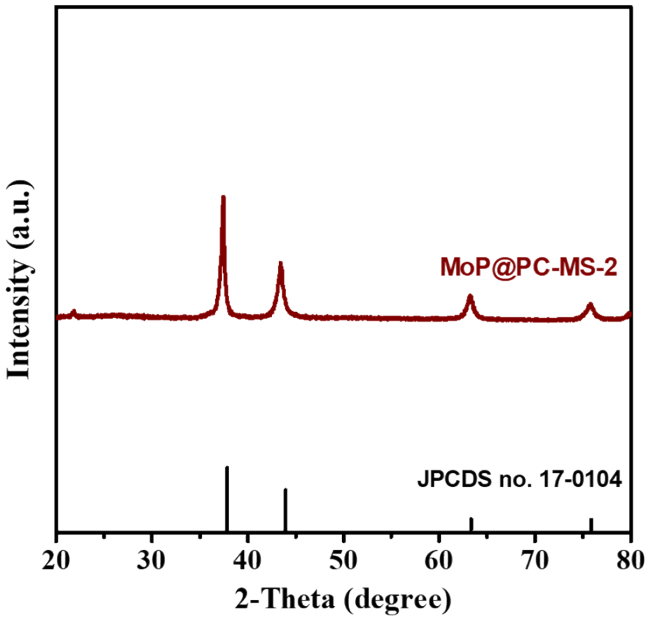

Figure S3. XRD pattern of MoP@PC-MS-2.

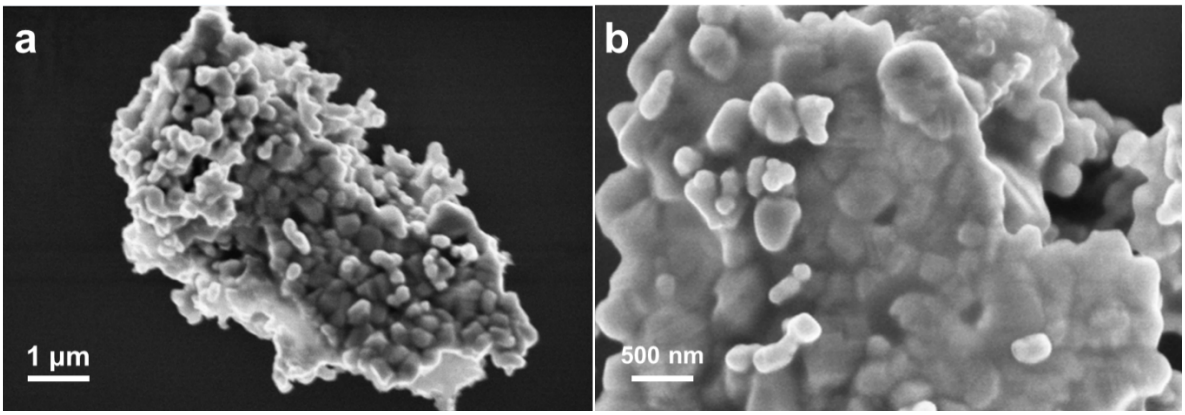

Figure S4. (a-b) SEM images of MoP@PC.

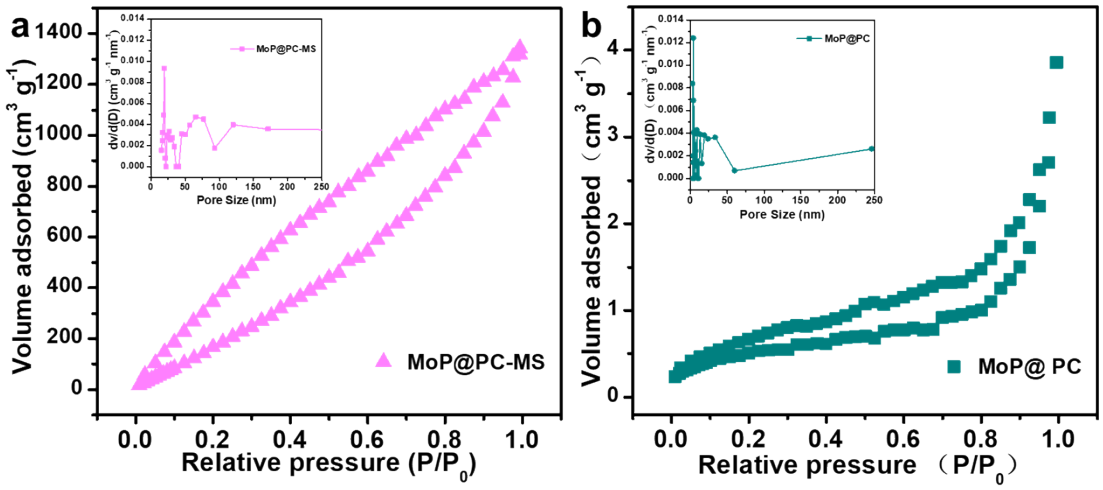

Figure S5. Nitrogen adsorption-desorption isotherms and pore size distribution of (a) MoP@PC-MS and (b) MoP@PC.

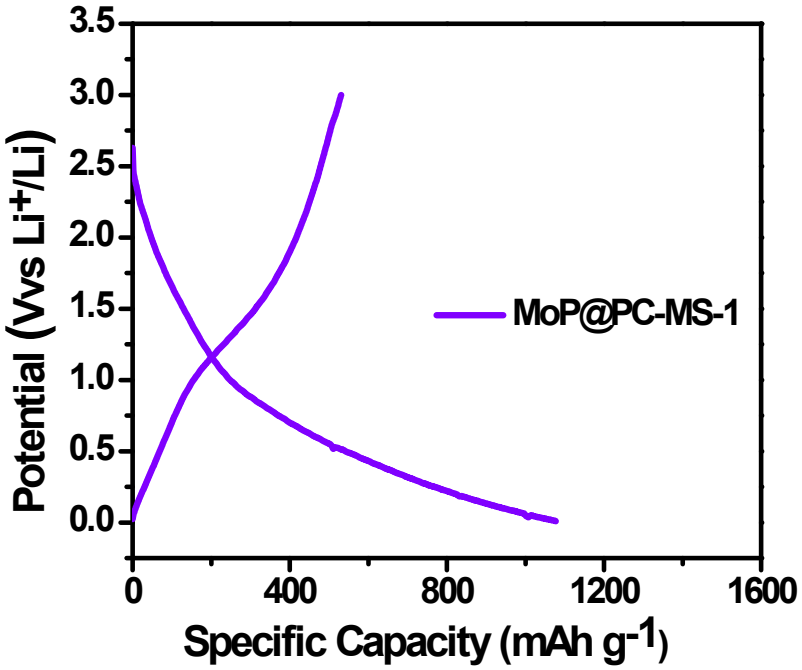

Figure S6. Charge-discharge curve of MoP@PC-MS-1.

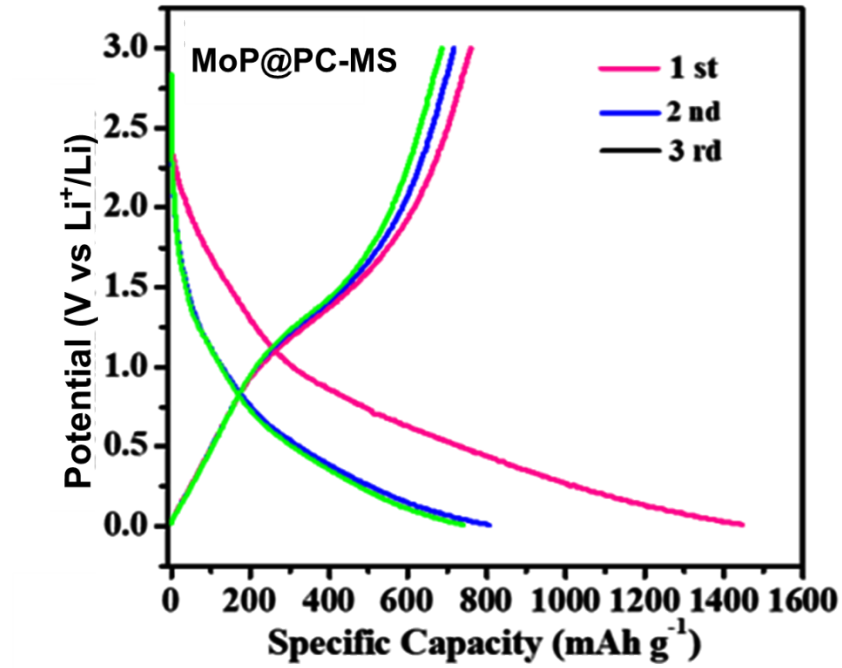

Figure S7. Charge-discharge curve of MoP@PC-MS at 0.05 A g^{-1}.

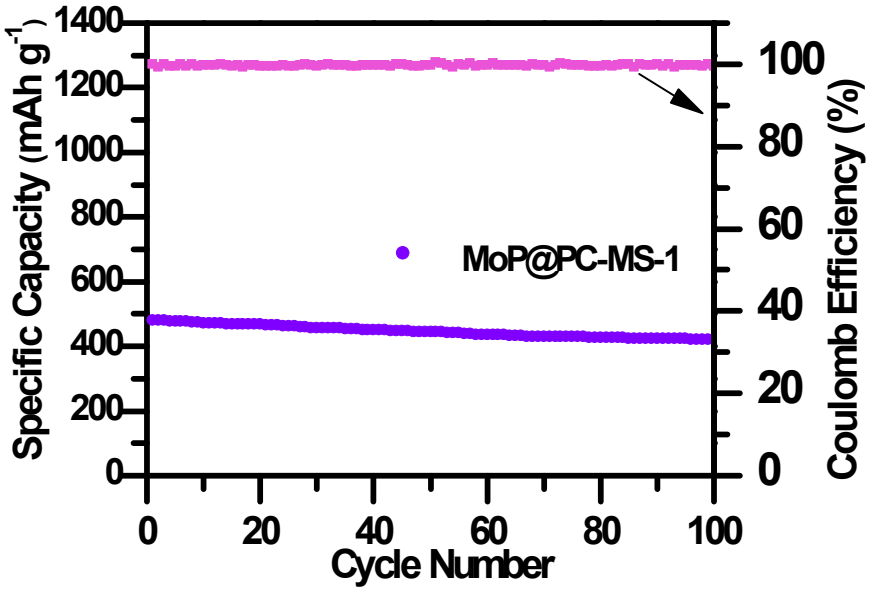

Figure S8. Cyclic performance of MoP@PC-MS-1.

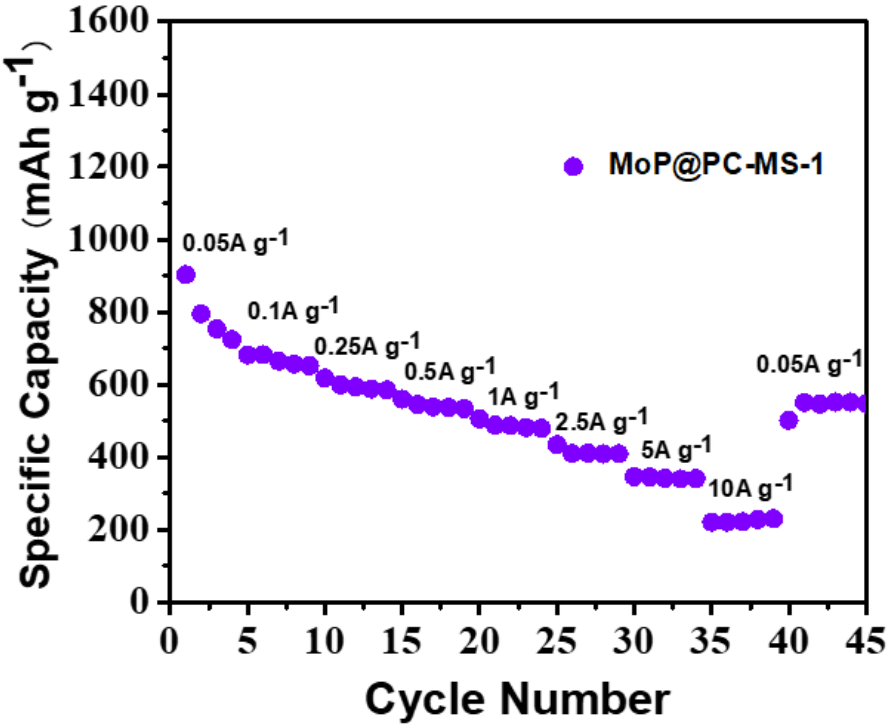

Figure S9. The rate performance of MoP@PC-MS-1.

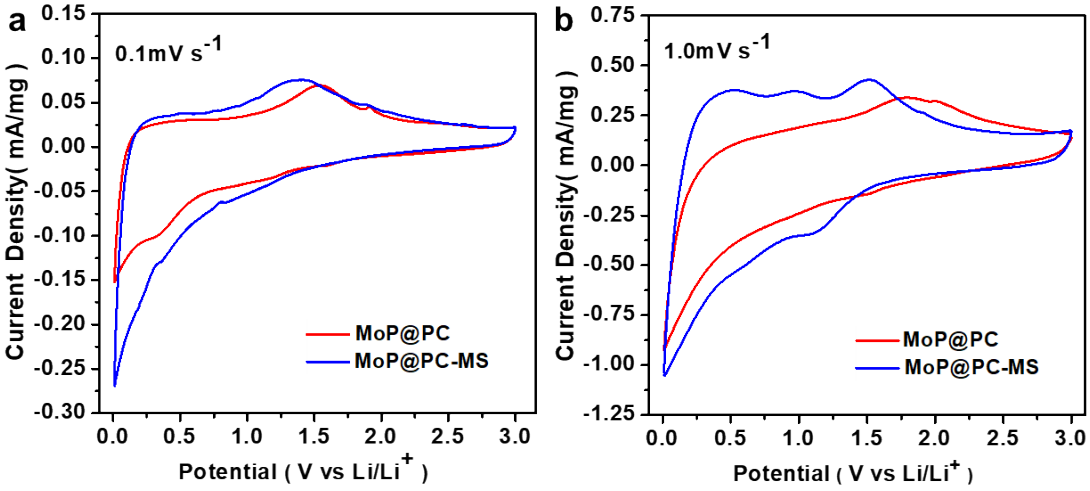

Figure S10. CV curves at 0.1mV s^{-1} and 1.0mV s^{-1} speeds of MoP@PC and MoP@PC-MS.

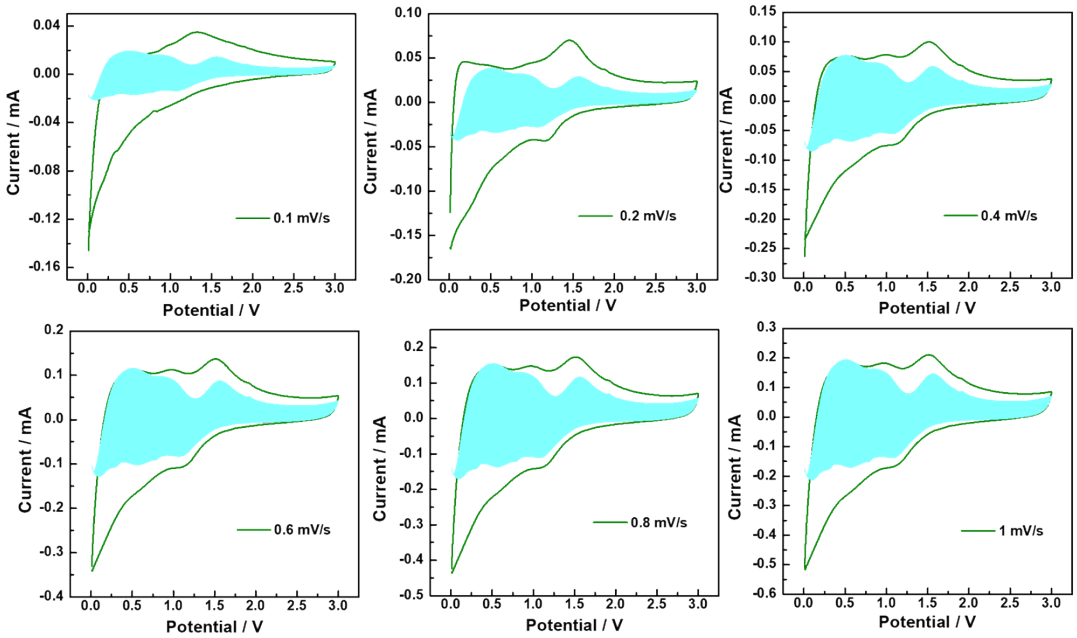

Figure S11. CV curves at different sweep speeds of MoP@PC-MS.